

Brief Papers

Experimental Validation of Nonlinear Control for a Voltage Source Converter

Edward Song, *Student Member, IEEE*, Alan F. Lynch, *Member, IEEE*, and Venkata Dinavahi, *Member, IEEE*

Abstract—In this brief, we consider reactive power and dc voltage tracking control of a three-phase voltage source converter (VSC). This control problem is important in many power system applications including power factor correction for a distribution static synchronous compensator (D-STATCOM). Traditional approaches to this problem are often based on a linearized model of the VSC and proportional-integral (PI) feedback. In order to improve performance, a flatness-based tracking control for the VSC is proposed where the nonlinear model is directly compensated without a linear approximation. Flatness leads to straightforward open-loop control design. A full experimental validation is given as well as a comparison with the industry-standard decoupled vector control. Robustness of the flatness-based control is investigated and setpoint regulation for unbalanced three-phase voltage is considered.

Index Terms—Nonlinear control, power systems, real-time control, voltage source converter (VSC).

I. INTRODUCTION

A VOLTAGE source converter (VSC) is an essential power electronic device with many applications in power systems. One such application is the distribution static synchronous compensator (D-STATCOM) which is used for power factor correction in power transmission and delivery. Power factor correction is an important issue in power delivery as it enables optimum power transfer to the load and minimum power loss to the electric utility. The STATCOM performs power factor correction by supplying or absorbing the reactive power demand (i.e., the reactive current demand) at the load bus. This minimizes the phase shift between the voltage and current which maximizes power factor. Tracking control of the STATCOM's reactive current while regulating its dc voltage is therefore a key performance objective.

Original work on controlling a VSC is in [1] where a decoupled d-q vector control using proportional-integral (PI) compensators was proposed. This work established a commonly used cascade controller structure for the real current and dc voltage where the PI control for the real current is contained inside the PI control for dc voltage. The reactive current is independently controlled by a separate PI controller. This control is based on a linearized averaged model of a VSC which accounts for the

fundamental components of the switching voltages. Exact modeling of the VSC has been considered in [2].

As the averaged model of the VSC is nonlinear, it is natural to apply model-based nonlinear control strategies which directly compensate for system nonlinearity without requiring a linear approximation. By avoiding approximation, nonlinear control can provide consistently high performance over a broad operating range. Nonlinear control of the VSC was first presented in [3] where state feedback linearization was applied with the linearizing output having dc voltage and reactive current as its components. Evidently, the result in [3] contains an error as this output does not state feedback linearize the system as claimed in the paper. More recently a number of authors have reconsidered input-output linearization using a number of simple tracking outputs [4]. In this last work, it is shown that choosing reactive current and dc voltage as the tracking output (as in [3]), the resulting zero dynamics are not stable. On the other hand, taking reactive and direct current as the output leads to an input output linearization with stable zero dynamics. The zero dynamics convergence suffers from parameter uncertainty and an uncontrolled and slow rate of convergence. To address these problems and assuming the direct current has very fast convergence to its desired value, a PI control for the reference value of the direct current is used to control the dc voltage. Earlier work in [5] uses the d -axis (real) current and dc voltage as a tracking output and is able to state feedback linearize provided they simplify the dc voltage dynamics by assuming line and switching losses are negligible. More recently, it became evident that this simplification is not required to achieve state feedback linearization [6]. Relative to the existing work on input output linearization [4], state feedback linearization has the advantage of linearizing the entire system dynamics which in turn leads to a mathematically elegant stability proof and simple control law. The work in [6] is the first application of differential flatness to the VSC. It demonstrates that by choosing a flat output as the reactive current and the energy stored in the system, the system can be fully linearized without zero dynamics. The flat output components can be interpreted as the lead components of the state feedback linearizing coordinate transformation. Unlike state feedback linearization, the flatness framework is natural for achieving trajectory planning. In [6], the objective is to track d -axis current and regulate dc voltage, and a load observer is used to avoid measuring the constant load. Although this work demonstrates the theory with simulation results, it does not experimentally validate the method's performance. In this brief, we address this issue and give experimental results for a flatness-based control. The control is also compared with a traditional PI cascade [1]. This brief also

Manuscript received May 01, 2007; Manuscript received in final form May 27, 2008. First published June 30, 2009; current version published August 26, 2009. Recommended by Associate Editor A. Bazanella.

E. Song is with the Department of Electrical and Computer Engineering, Louisiana State University, Baton Rouge, LA 70803 USA.

A.F. Lynch and V. Dinavahi are with the Department of Electrical and Computer Engineering, University of Alberta, Edmonton AB T6G 2V4, Canada.

Color versions of one or more of the figures in this brief are available online at <http://ieeexplore.ieee.org>.

Digital Object Identifier 10.1109/TCST.2008.2001741



Fig. 1. University of Alberta Powerex VSC system.

illustrates the well known benefit of flatness for achieving motion planning in order to steer the system between two operating points while respecting system constraints. Unlike in [6], in this brief we focus on the STATCOM application where no load is present on the dc side (floating dc capacitor), and the objective is to track dc voltage and reactive current. Hence, the novelty of the work in this brief is its experimental nature and its focus on the VSC for a STATCOM application. The experiments were performed on a VSC test bed in the real-time experimental laboratory (RTX-LAB) at the University of Alberta.

This brief is structured as follows. Section II provides a description of the test stand. Section III presents the averaged nonlinear VSC model. In Section IV, a flatness-based open-loop motion planning and closed-loop tracking controller is presented. Section V gives details on the implementation of the PWM scheme. Experimental performance of the nonlinear control is presented in Section VI.

II. VSC SYSTEM TEST STAND

We consider a six-pulse insulated gate bipolar transistor (IGBT)-based VSC driven by a sinusoidal pulse-width modulation scheme (sine PWM). The VSC is connected to a three-phase ac voltage supply with filter inductors. Fig. 1 shows the actual VSC used for the experiment. An ac supply provides a 60 Hz three-phase sinusoidal voltage with a peak line-to-neutral voltage of $\hat{V} = 100\sqrt{2/3}$ V which is equivalent to a line-to-line RMS voltage of 100 V. The VSC was manufactured by *Powerex Inc.* (model number: PP75T060) [7]. The converter consists of six IGBTs and six anti-parallel diodes. The capacitor bank contains large resistances R_c connected in parallel so that the capacitors can be gradually discharged by themselves for safety purpose. Although the current and voltage ratings of the VSC are 75 A and 600 V, respectively, the circuit breaker is rated for 20 A. The gate drive board is mounted on the top of the converter and is responsible for sending the six digital gating pulses as well as for measuring various signals such as heat sink temperature, three-phase currents, and dc voltage. The gate drive board contains $2 \mu\text{s}$ of dead time [8]. The three-phase ac currents are measured by LEM Hall-effect sensors.

A real-time digital simulator manufactured by *Opal-RT Technologies Inc.* is used for the controller hardware [9]. The simulator

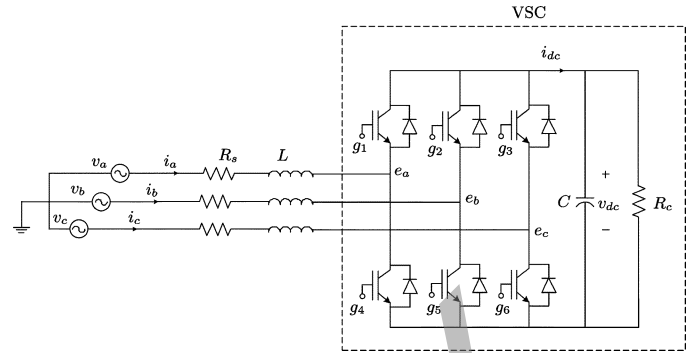


Fig. 2. Circuit diagram of the experimental setup.

TABLE I
MODEL PARAMETERS

parameter	value	units
R_s	0.3	Ω
R_c	18000	Ω
L	0.0025	H
C	0.0033	F
ω	120π	rad/s
\hat{V}	$100\sqrt{2/3}$	V

uses a dual-Intel Xeon processor to evaluate the control algorithm. Conventionally, less general purpose DSP-based hardware is used to implement a controller. However, the Opal-RT simulator provides the benefit of a flexible controller development environment with more than sufficient computing capability for a wide variety of applications. The simulator also houses a Xilinx Virtex II Pro field-programmable gate-array (FPGA) device which was programmed for pulse-width-modulation (PWM) generation. The FPGA contains 11 088 logic cells and runs on a 100-MHz clock cycle which leads to a 10 ns time step.

III. MATHEMATICAL MODEL

The circuit diagram for the VSC system is shown in Fig. 2. This configuration is a typical setup for STATCOM applications [10], [11]. The three-phase ac voltage supply v_a, v_b, v_c is connected to the ac terminals of the VSC through an inductance L which models a transformer (not shown in Fig. 2) leakage inductance and filter inductance. The terminal voltages of the VSC are denoted e_a, e_b, e_c . Although it is desired to have a balanced three-phase ac supply, we allow for an unbalance of the form

$$\begin{aligned} v_a &= \hat{V}_a \cos(\omega t) \\ v_b &= \hat{V}_b \cos\left(\omega t - 2\frac{\pi}{3} + \phi_b\right) \\ v_c &= \hat{V}_c \cos\left(\omega t + 2\frac{\pi}{3} + \phi_c\right) \end{aligned}$$

where $\hat{V}_a, \hat{V}_b, \hat{V}_c$ are not necessarily equal to the nominal line to neutral voltage \hat{V} and ϕ_b, ϕ_c can be nonzero phase shifts. The gating signals g_1, \dots, g_6 are binary-valued inputs to the IGBT switches where a 1 and 0 indicate a closed and open configuration, respectively. These gating signals are directly fed from the outputs of the sine PWM pulse generator. The line losses and the transformer conduction losses are modelled by R_s , and the inverter switching losses are modelled by the shunt resistance [1] which is lumped with the capacitor bank resistance R_c . The system parameters for the experimental setup are provided in Table I.

Details on the modeling of the three-phase VSC system are in [1]. The dynamics in a synchronously rotating d - q frame are

$$\begin{aligned} \frac{di_d}{dt} &= -\frac{R_s}{L}i_d + \omega i_q + \frac{v_d}{L} - \frac{e_d}{L}, & e_d &= \frac{1}{2}v_{dc}m_a \cos \delta \\ \frac{di_q}{dt} &= -\frac{R_s}{L}i_q - \omega i_d + \frac{v_q}{L} - \frac{e_q}{L}, & e_q &= \frac{1}{2}v_{dc}m_a \sin \delta \\ \frac{dv_{dc}}{dt} &= \frac{3}{2} \frac{e_d i_d + e_q i_q}{Cv_{dc}} - \frac{v_{dc}}{CR_c} \end{aligned} \quad (1)$$

where i_d, i_q are the d, q components of the currents i_a, i_b, i_c , and e_d, e_q are the d, q components of the VSC terminal voltages e_a, e_b, e_c , and m_a, δ are the physical controller outputs to the system and denote the modulation index and the phase shift of the sine PWM, respectively [12]. Since v_a, v_b, v_c is unbalanced, their representation in the d - q frame v_d, v_q can be time in general. The expression for v_d is

$$\begin{aligned} v_d &= \frac{2}{3} \left(\hat{V}_a \cos^2(\omega t) + \hat{V}_b \cos\left(\omega t - \frac{2\pi}{3} + \phi_b\right) \cos\left(\omega t - \frac{2\pi}{3}\right) \right. \\ &\quad \left. + \hat{V}_c \cos\left(\omega t + \frac{2\pi}{3} + \phi_c\right) \cos\left(\omega t + \frac{2\pi}{3}\right) \right) \end{aligned}$$

which can be simplified into

$$v_d = V_{d1} + V_{d2} \cos(2\omega t) + V_{d3} \sin(2\omega t) \quad (2)$$

where $V_{d1} = \hat{V}_a/3 + (\hat{V}_b/3) \cos \phi_b + (\hat{V}_c/3) \cos \phi_c$, $V_{d2} = \hat{V}_a/3 + (\hat{V}_b/3) \cos(\phi_b - 4\pi/3) + (\hat{V}_c/3) \cos(\phi_c + 4\pi/3)$, $V_{d3} = -(\hat{V}_b/3) \sin(\phi_b - 4\pi/3) - (\hat{V}_c/3) \sin(\phi_c + 4\pi/3)$. Similarly, we have

$$v_q = V_{q1} - V_{q2} \cos(2\omega t) - V_{q3} \sin(2\omega t) \quad (3)$$

with $V_{q1} = (\hat{V}_b/3) \sin \phi_b + (\hat{V}_c/3) \sin \phi_c$, $V_{q2} = (\hat{V}_b/3) \sin(\phi_b - 4\pi/3) + (\hat{V}_c/3) \sin(\phi_c + 4\pi/3)$, $V_{q3} = \hat{V}_a/3 + (\hat{V}_b/3) \cos(\phi_b - 4\pi/3) + (\hat{V}_c/3) \cos(\phi_c + 4\pi/3)$. Note that in the unbalanced case, v_d and v_q contain second order harmonic components. We also note that for a balanced three-phase source, i.e., $\hat{V}_a = \hat{V}_b = \hat{V}_c = \hat{V}$ and $\phi_b = \phi_c = 0$, (2) and (3) simplify to the constants $v_d = \hat{V}$, $v_q = 0$. In the following, we drop the argument of time for v_d and v_q to simplify notation. If we choose the state $x = (x_1, x_2, x_3)^T = (i_d, i_q, v_{dc})^T$ and input $u = (u_1, u_2)^T = (m_a \cos \delta, m_a \sin \delta)^T$, then the system's dynamics in state space form are

$$\dot{x} = f(x, t) + g_1(x)u_1 + g_2(x)u_2 \quad (4)$$

where

$$\begin{aligned} f(x, t) &= \left[\frac{v_d}{L} - \frac{R_s}{L}x_1 + \omega x_2, \frac{v_q}{L} - \omega x_1 - \frac{R_s}{L}x_2, -\frac{x_3}{CR_c} \right]^T \\ g_1(x) &= \left[-\frac{x_3}{2L}, 0, \frac{3x_1}{4C} \right]^T \\ g_2(x) &= \left[0, -\frac{x_3}{2L}, \frac{3x_2}{4C} \right]^T. \end{aligned}$$

We remark that since $0 \leq m_a \leq 1$, $-\pi/2 \leq \delta \leq \pi/2$ this is equivalent to $0 \leq u_1 \leq 1, u_1^2 + u_2^2 \leq 1$. Also, we remark that (4) is time varying when the source is not balanced.

IV. FLATNESS-BASED TRAJECTORY TRACKING

A. Feedback Linearization

The relation between feedback linearization and differential flatness is well known [13]. In this brief, we make use of both notions as system (4) is locally static state feedback linearizable, and this allows us to systematically determine a flat output. Flatness is then used to design an open-loop control which steers the system between equilibrium points while respecting constraints on the input. It is interesting to remark that any system with $(m+1)$ -dimensional state and m -inputs is flat if and only if it is controllable [14]. Since the VSC is controllable and has three states and two inputs, it is necessarily flat and dynamically feedback linearizable using endogenous feedback. Although (4) is time varying, the conditions for local static state feedback linearizability of the system can be found in [15]. System (4) is locally static state feedback linearizable about $x_0 \in \mathbb{R}^3$ if and only if it follows:

- 1) distribution $\mathcal{G}_0 = \text{span}\{g_1, g_2\}$ is involutive and constant rank equal to 2;
- 2) the rank of distribution $\mathcal{G}_1 = \text{span}\{g_1, g_2, \text{ad}_f g_1, \text{ad}_f g_2\}$ is 3 for all time.

Clearly \mathcal{G}_0 is involutive and constant rank equal to 2 provided $x_3 \neq 0$. The rank of \mathcal{G}_1 is 3 except when $x_3 = 0$ or

$$\bar{x}_1 = \frac{-CR_c v_d}{2\sigma}, \quad \bar{x}_2 = \frac{-CR_c v_q}{2\sigma} \quad (5)$$

where $\sigma = L - CR_c R_s$. In practice, the current \bar{x}_1 is far from any realistic operating condition and therefore does not limit the domain on which the system is linearizable. For example, substituting parameters from Table I and assuming a balanced source gives $\bar{x}_1 = 136.1$ A, and we require that current amplitude not exceed 20 A in our system. For convenience we define a practical domain on which the system is feedback linearizable: $\mathbf{S} = \{x \in \mathbb{R}^3 : x_1 < \bar{x}_1; x_3 > 0\}$. The linearizing state coordinates are $z_1 = \varphi_1(x)$, $z_2 = L_f \varphi_1(x, t)$, $z_3 = \varphi_2(x)$ and for nonzero $d\varphi_1 \in \mathcal{G}_0^\perp$, i.e., $\langle d\varphi_1, g_k \rangle = 0, k = 1, 2$. The choice of φ_2 is discussed below. Using Maple's `pdesolve`, we obtain

$$\varphi_1(x) = \gamma \left(\frac{3L}{2C} (x_1^2 + x_2^2) + x_3^2 \right) + c \quad (6)$$

where γ is some C^1 function, and c is some constant. A physically relevant choice for φ_1 is the sum of the energy stored in the inductors E_L and the capacitor E_C

$$E_L = \frac{1}{2}L(i_a^2 + i_b^2 + i_c^2) = \frac{3}{4}L(i_d^2 + i_q^2), \quad E_C = \frac{1}{2}Cv_{dc}^2.$$

Hence, we choose

$$\varphi_1(x) = E_L + E_C = \frac{3}{4}L(x_1^2 + x_2^2) + \frac{1}{2}Cx_3^2.$$

Work in [6] uses the same flat output component but does not derive it from the necessary condition for static state feedback

linearization: $\langle d\varphi_1, g_k \rangle = 0$, $k = 1, 2$. In that work, physical reasoning leads to the choice of φ_1 . That is, knowing the energy and power dissipation of the system, and i_q allows us to uniquely determine all system variables. An advantage of using the condition $\langle d\varphi_1, g_k \rangle = 0$, $k = 1, 2$ for selecting φ_1 is its systematic nature.

The function φ_2 is chosen independent of φ_1 and $L_f\varphi_1$ on \mathbf{S} , and such that the decoupling matrix

$$F(x, t) = \begin{bmatrix} L_{g_1}L_f\varphi_1 & L_{g_2}L_f\varphi_1 \\ L_{g_1}\varphi_2 & L_{g_2}\varphi_2 \end{bmatrix}$$

is nonsingular on \mathbf{S} . This existence of such a φ_2 is guaranteed by the conditions for linearization. The choice $\varphi_2(x) = x_2$ yields a coordinate transformation shown in (7) at the bottom of the page, which is well-defined on \mathbf{S} for any time. As well, the matrix F is nonsingular on all of \mathbf{S} for any time. We remark that the particular choice of φ_2 is convenient as it simplifies trajectory planning since we wish to directly control the reactive current x_2 . Also, z_2 , being equal to the time derivative of z_1 , is the net power into the system.

B. Flatness

Static state feedback linearizable systems are flat with the flat output being the lead components of the coordinate transformation for each input, i.e.,

$$y_1(x) = \varphi_1(x) = \frac{3}{4}L(x_1^2 + x_2^2) + \frac{1}{2}Cx_3^2, \quad y_2(x) = \varphi_2(x) = x_2 \quad (8)$$

where y_1, y_2 denote the components of the flat output. We can express the states as functions of the flat output and its derivatives. For our system, we have (9), shown at the bottom of the page, where (10), shown at the bottom of the page, holds, and $\zeta(y, \dot{y}, t) = CR_c(8R_s^2y_1 + L(4R_s\dot{y}_1 - 3v_d^2 - 6R_s v_q y_2))$. The input expressed as functions of the flat output and its time derivatives is shown in (11) at the bottom of the page, where $\beta(t) = 3(\dot{v}_d x_1 + \dot{v}_q x_2)/2$, $v_{dq} = v_d^2 + v_q^2$, $x_{12} = x_1^2 + x_2^2$ and expressions for x in terms of y and \dot{y} (i.e., (9)) can be substituted. We remark that the flat outputs are closely related to variables we want to influence: i_q and v_{dc} . This is because energy stored in the capacitor is much larger than that in the inductors. Hence, tracking energy is similar to tracking v_{dc} .

C. Open-Loop Motion Planning

We consider a motion planning problem where we move the system between two equilibrium states $x_0 = (\dot{i}_{do}, \dot{i}_{qo}, v_{dco})^\top$ and $x_1 = (\dot{i}_{d1}, \dot{i}_{q1}, v_{dc1})^\top$. The solution to this problem is to find a control u , defined on $[t_o, t_1]$ so that $x(t_o) = x_0$ and $x(t_1) = x_1$. Such a motion planning problem for a flat system can be readily solved and can be reduced to solving a linear system of equations. This is because the flat output trajectory $y(t)$ must satisfy

$$\begin{aligned} x_1 &= \mathcal{A}(y_1(t_0), \dot{y}_1(t_0), y_2(t_0), t_0) \\ x_2 &= \mathcal{A}(y_1(t_1), \dot{y}_1(t_1), y_2(t_1), t_1) \end{aligned} \quad (12)$$

where \mathcal{A} is given in (9). Conditions (12) impose constraints on $y(t)$, $\dot{y}(t)$, $\ddot{y}(t)$ at the endpoints $t = t_0$ and $t = t_1$. In order to design a flat output trajectory that satisfies the above constraints,

$$(z_1, z_2, z_3) = (\varphi_1(x), L_f\varphi_1(x, t), \varphi_2(x)) = \left(\frac{3}{4}L(x_1^2 + x_2^2) + \frac{1}{2}Cx_3^2, \frac{3R_c(v_d x_1 + v_q x_2 - R_s(x_1^2 + x_2^2)) - 2x_3^2}{2R_c}, x_2 \right) \quad (7)$$

$$x = \mathcal{A}(y_1, \dot{y}_1, y_2, t) = \left(\frac{\psi(y, \dot{y}, t) - 3CR_c v_d}{6\sigma}, y_2, \frac{\sqrt{R_c \zeta(y, \dot{y}, t) - LR_c(8R_s y_1 + 4L\dot{y}_1 - 6Lv_q y_2 - v_d \psi(y, \dot{y}))}}{2\sigma} \right) \quad (9)$$

$$\psi(y, \dot{y}, t) = (9C^2 R_c^2 v_d^2 + 12\sigma(4y_1 - 3Ly_2^2 + CR_c(2\dot{y}_1 - 3y_2(v_q - R_s y_2))))^{1/2} \quad (10)$$

$$\begin{aligned} u &= \mathcal{B}(y_1, \dot{y}_1, \ddot{y}_1, y_2, \dot{y}_2, t) = F^{-1}(x, t) \begin{bmatrix} \ddot{y}_1 - L_f^2 \varphi_1(x, t) - \beta(t) \\ \dot{y}_2 - L_f \varphi_2(x, t) \end{bmatrix} \\ &= \begin{bmatrix} \frac{-4CLR_c}{x_3(3CR_c v_d + 6x_1 \sigma)} & \frac{2L(2x_2 \sigma + CR_c v_q)}{x_3(2x_1 \sigma + CR_c v_d)} \\ 0 & -\frac{2L}{x_3} \end{bmatrix} \times \begin{bmatrix} \dot{y}_1 - \frac{3(v_{dq} - v_q(\omega L x_1 + 3R_s x_2) + v_d(\omega L x_2 - 3R_s x_1) + 2R_s^2 x_{12})}{2L} - \frac{2x_3^2}{CR_c^2} - \beta(t) \\ \dot{y}_2 + \omega x_1 + \frac{R_s}{L} x_2 - \frac{v_q}{L} \end{bmatrix} \quad (11) \end{aligned}$$

we parameterize the components of y_1, y_2 in terms of polynomial basis functions

$$y_i(t) = \sum_{j=0}^{N_i} \frac{a_{ij}}{j!} (t - t_o)^j, \quad i = 1, 2.$$

Hence, we have (13) shown at the bottom of the page. The motion planning constraints at the end points are

$$\begin{aligned} y_1(t_o) &= \frac{1}{2}Cv_{dco}^2 + \frac{3}{4}L(i_{do}^2 + i_{qo}^2) \\ y_1(t_1) &= \frac{1}{2}Cv_{dc1}^2 + \frac{3}{4}L(i_{d1}^2 + i_{q1}^2) \\ \dot{y}_1(t_o) &= 0, \quad \dot{y}_1(t_1) = 0, \quad \ddot{y}_1(t_o) = 0, \quad \ddot{y}_1(t_1) = 0 \\ y_2(t_o) &= i_{qo}, \quad y_2(t_1) = i_{q1}, \quad \dot{y}_2(t_o) = 0, \quad \dot{y}_2(t_1) = 0. \end{aligned}$$

These relations give six conditions on y_1 and four conditions on y_2 . Expressions for some of the coefficients are immediately obtained

$$\begin{aligned} a_{10} &= y_1(t_o) = \frac{1}{2}Cv_{dco}^2 + \frac{3}{4}Li_{qo}^2 \\ a_{11} &= \dot{y}_1(t_o) = 0 \\ a_{12} &= \ddot{y}_1(t_o) = 0 \\ a_{20} &= y_2(t_o) = i_{qo} \\ a_{21} &= \dot{y}_2(t_o) = 0. \end{aligned}$$

Up to now we have imposed six constraints on y_1 . We choose the degree $N_1 = 8$ to meet additional constraints on input and state as discussed below. We can express a_{10}, \dots, a_{15} in terms of the remaining three coefficients. Similarly, choosing $N_2 = 7$, we can express a_{20}, \dots, a_{23} in terms of the remaining four coefficients. We have (14) shown at the bottom of the page, where $\Delta t = t_1 - t_o$. Next, by varying the remaining coefficients a_{16}, a_{17}, a_{18} and a_{24}, a_{25}, a_{26} we can ensure system variables are

restricted to a practical region. For example, the currents should not exceed the maximum current rating of the circuit breaker. To illustrate the approach, we consider the following specific constraints:

- 1) $(i_{q0}, v_{dco}) = (-10 \text{ A}, 200 \text{ V})$ and $(i_{q1}, v_{dc1}) = (10 \text{ A}, 240 \text{ V})$.
- 2) *Input Constraints:* $0 \leq m_a(t) \leq 1, |\delta(t)| \leq \pi/2, t \in [t_0, t_1]$.
- 3) *Current Constraints:* $0 \text{ A} \leq i_d(t) \leq 20 \text{ A}, |i_q(t)| \leq 20 \text{ A}, t \in [t_0, t_1]$.

The transition time Δt should be as small as possible. To ensure Objectives 2 and 3 are satisfied, the remaining unconstrained coefficients of the flat output parameterizations are numerically optimized. MATLAB's `fseminf` function yields the desired flat output trajectories

$$\begin{aligned} y_{1,d}(t) &= 66.188 + 1.4 \cdot 10^7 t^3 - 1.7 \cdot 10^9 t^4 + 6.7 \cdot 10^{10} t^5 \\ y_{2,d}(t) &= -10 + 4.8 \cdot 10^4 t^2 - 1.92 \cdot 10^6 t^3 \end{aligned}$$

where $t_0 = 0$ and $t_1 = 50 \text{ ms}$.

D. Closed-Loop Tracking Control

To account for disturbances, model error, and initial tracking error, the open-loop control must be augmented with state feedback. We define the components of the tracking error as

$$\begin{aligned} e_1(t) &= \int_0^t (y_1(\tau) - y_{1,d}(\tau)) d\tau \\ e_2(t) &= y_1(t) - y_{1,d}(t) \\ e_3(t) &= \frac{dy_1}{dt}(t) - \frac{dy_{1,d}}{dt}(t) \\ e_4(t) &= \int_0^t (y_2(\tau) - y_{2,d}(\tau)) d\tau \\ e_5(t) &= y_2(t) - y_{2,d}(t) \end{aligned}$$

$$\begin{bmatrix} 1 & t - t_o & \frac{(t-t_o)^2}{2!} & \dots & \frac{(t-t_o)^{N_i-1}}{(N_i-1)!} & \frac{(t-t_o)^{N_i}}{N_i!} \\ 0 & 1 & t - t_o & \dots & \frac{(t-t_o)^{N_i-2}}{(N_i-2)!} & \frac{(t-t_o)^{N_i-1}}{(N_i-1)!} \\ \vdots & \vdots & \vdots & \ddots & \vdots & \vdots \\ 0 & 0 & 0 & \dots & 1 & t - t_o \\ 0 & 0 & 0 & \dots & 0 & 1 \end{bmatrix} \begin{bmatrix} a_{i0} \\ a_{i1} \\ \vdots \\ a_{iN_i} \end{bmatrix} = \begin{bmatrix} y_i(t) \\ \dot{y}_i(t) \\ \vdots \\ y_i^{(N_i)}(t) \end{bmatrix} \quad (13)$$

$$\begin{aligned} a_{13} &= -\frac{\Delta t^6(28a_{16} + 3\Delta t(4a_{17} + a_{18})) + 50400(3(i_{qo} - i_{q1})(i_{qo} + i_{q1})L + 2C(v_{dco} - v_{dc1})(v_{dco} + v_{dc1}))}{3360\Delta t^3} \\ a_{14} &= \frac{168a_{16}\Delta t^6 + \Delta t^7(64a_{17} + 15a_{18}\Delta t) + 151200(3(i_{qo} - i_{q1})(i_{qo} + i_{q1})L + 2C(v_{dco} - v_{dc1})(v_{dco} + v_{dc1}))}{1680\Delta t^4} \\ a_{15} &= -\frac{84a_{16}\Delta t^6 + \Delta t^7(24a_{17} + 5a_{18}\Delta t) + 30240(3(i_{qo} - i_{q1})(i_{qo} + i_{q1})L + 2C(v_{dco} - v_{dc1})(v_{dco} + v_{dc1}))}{168\Delta t^5} \\ a_{22} &= \frac{210a_{24}\Delta t^4 + 84a_{25}\Delta t^5 + 21a_{26}\Delta t^6 + 4a_{27}\Delta t^7 - 15120(i_{qo} - i_{q1})}{2520\Delta t^2} \\ a_{23} &= \frac{10080(i_{qo} - i_{q1}) - 420a_{24}\Delta t^4 - 126a_{25}\Delta t^5 - 28a_{26}\Delta t^6 - 5a_{27}\Delta t^7}{840\Delta t^3} \end{aligned} \quad (14)$$

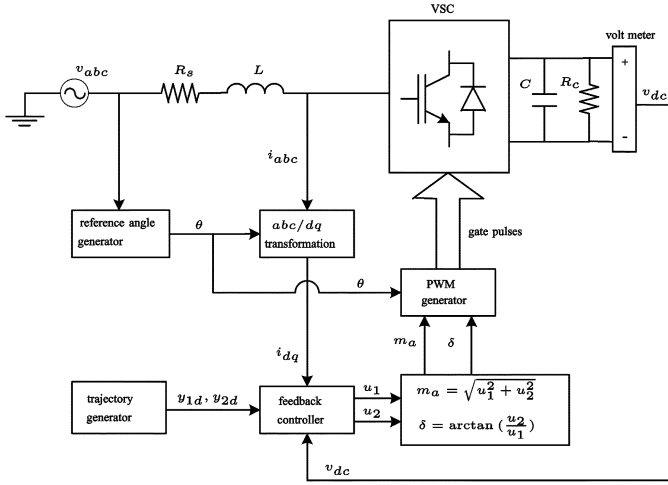


Fig. 3. Flatness-based control scheme for the VSC-based STATCOM system.

where $y_{1,d}$, $y_{2,d}$ denotes the desired flat output trajectories designed in the previous section. The state feedback control is

$$u = F^{-1}(x, t) \begin{bmatrix} \ddot{y}_{1,d} - k_1 e_1 - k_2 e_2 - k_3 e_3 - L_f^2 \varphi_1 - \beta(t) \\ \ddot{y}_{2,d} - k_4 e_4 - k_5 e_5 - L_f \varphi_2 \end{bmatrix}. \quad (15)$$

Static state feedback (15) yields a fifth-order linear time-invariant tracking error dynamics whose equilibrium point is exponentially stable. The integral of the tracking error is included to reject the effects of constant disturbances. Fig. 3 illustrates the block diagram of the flatness-based control.

V. SINE PWM IMPLEMENTATION

In this section, we present the implementation details for the sine PWM scheme using an FPGA device. Fig. 4 shows a block diagram of the circuit. Other work which describes PWM generation using FPGAs is in [10]. The inputs to the VSC are the six gating pulses g_i provided by the PWM circuit. These pulses are a function of the modulation index m_a and phase shift δ which are computed from the control inputs u_1 and u_2 using (15). The digital simulator generates the modulating inputs to the PWM circuit

$$\begin{aligned} v_1 &= m_a \cos(\omega t + \delta) \\ v_2 &= m_a \cos\left(\omega t - \frac{2\pi}{3} + \delta\right) \\ v_3 &= m_a \cos\left(\omega t + \frac{2\pi}{3} + \delta\right). \end{aligned} \quad (16)$$

The PWM circuit consists of two main parts: a high frequency triangular carrier wave construction and pulse generation. The design is specifically implemented for the control sampling frequency of 4 kHz with a 2 kHz carrier frequency. The triangular carrier wave v_t has a period of 500 μ s. It is generated internally in the FPGA using a 16 bit counter. Since the FPGA has a clock period of 10 ns, the counter should count up from $-12\,500$ to $12\,500$ and then down to $-12\,500$ in 500 μ s. In order to synchronize the counter with the reference control signal, the digital simulator also needs to send a synchronizing signal, labeled *sync* in Fig. 4, to the FPGA in addition to the modulating inputs(16).

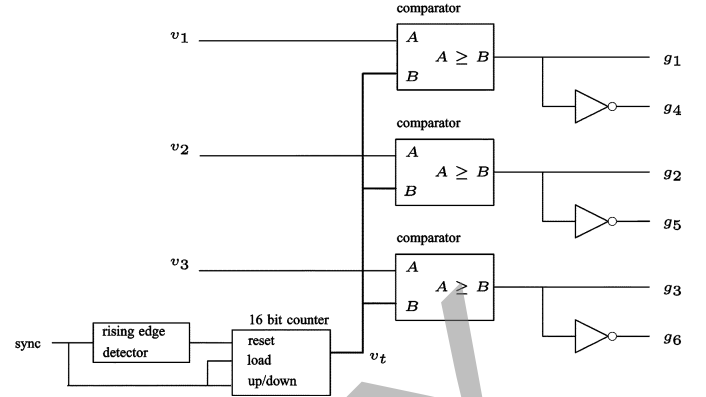


Fig. 4. Block diagram of sine PWM implemented in an FPGA.

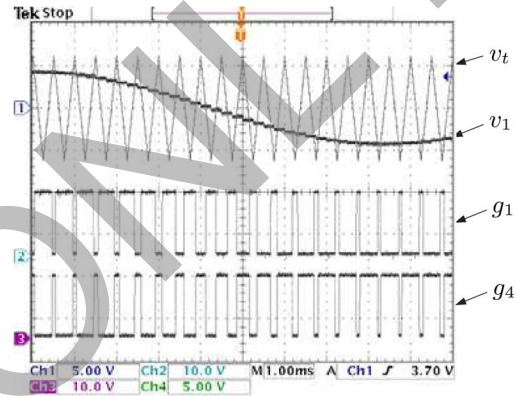


Fig. 5. Sine PWM Oscilloscope waveforms.

The *sync* signal is a pulse with 50% duty ratio and a frequency of 2 kHz. The counter requires a reset port which resets its output to the initial value of $-12\,500$ (on the rising edges of the *sync* signal), a load port which loads either $-12\,500$ (for rising edges of *sync*) or $12\,500$ (for falling edges of *sync*) at the output of the counter, and an up/down port (count up when *sync* is high and count down otherwise) which determines the direction of the counting. Although the amplitude of the modulating signals is 1 in the mathematical model, these signals are scaled by a factor of 12 500 in order to match the carrier signal amplitude used in practice. The gate pulses for the three upper switches g_1 , g_2 , g_3 come from the output of the comparators in the FPGA and the lower gate signals g_4 , g_5 , g_6 are the inverted signals of their respective upper switches. The Powerex inverter requires a minimum dead-time of 1.2 μ s. Since 2 μ s of dead-time is already built in the gate drive board of the converter, dead-time implementation is not required on the FPGA. Fig. 5 shows typical sine PWM waveforms of the upper switch (g_1) and lower switch (g_4) captured on an oscilloscope. Note that the time step of the sinusoidal modulating signal v_k is 250 μ s whereas the period of the carrier wave v_t is 500 μ s. The FPGA design was performed in MATLAB/Simulink using the Xilinx System Generator toolbox.

VI. EXPERIMENTAL RESULTS

A. Flatness-Based Control: Balanced Source

Fig. 6(a) and (b) show the experimental results of the flatness-based control using the particular open-loop trajectory de-

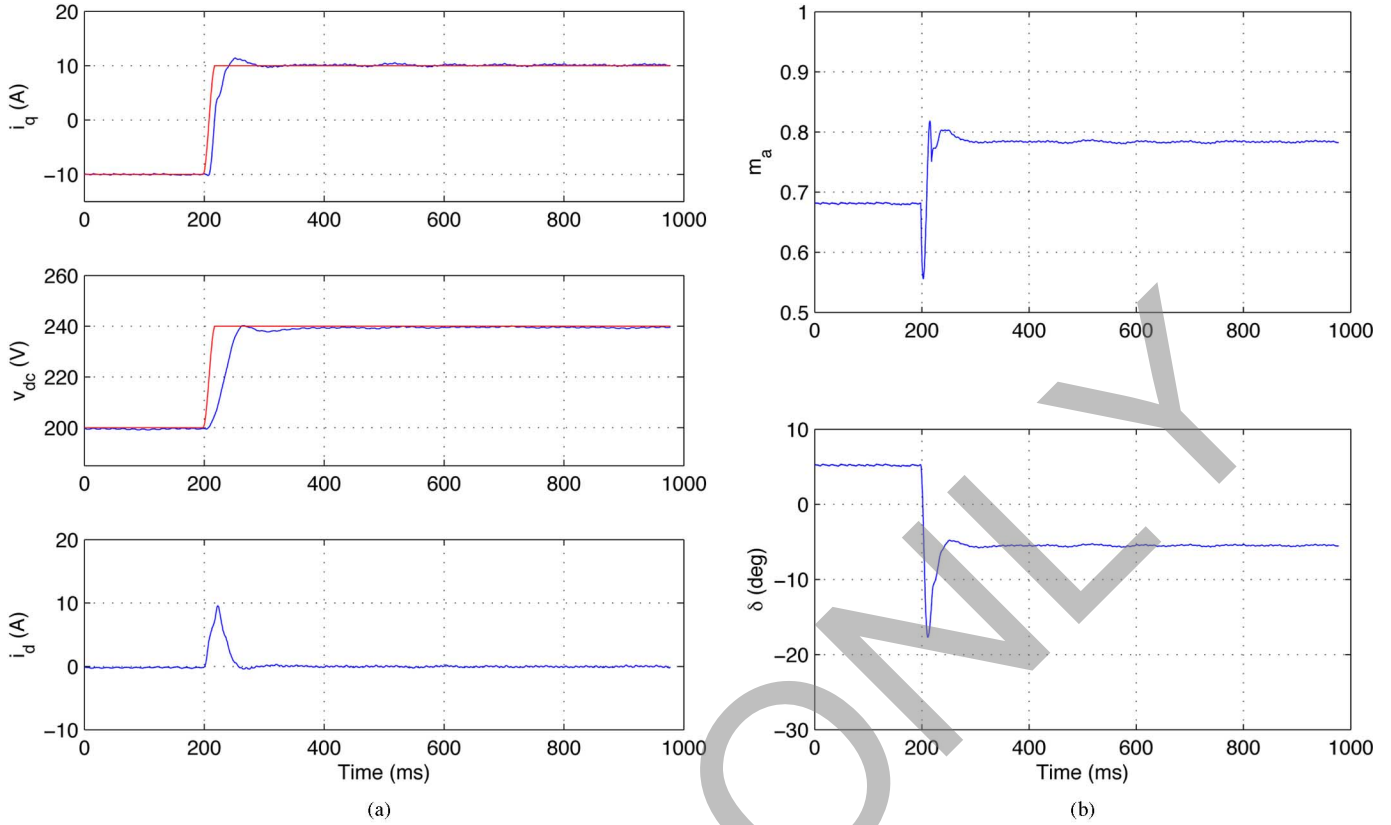


Fig. 6. Flatness-based control. (a) Trajectories of i_q , v_{dc} , and i_d . (b) Trajectories of m_a and δ .

signed in Section IV. The three-phase ac voltage source used for this experiment was assumed balanced. In practice, the ac source had a small amount of unmodelled harmonic content. The reference transition begins at $t = 150$ ms. The graphs in Fig. 6(a) show the reference or open-loop trajectories for i_q and v_{dc} . The actual closed-loop responses demonstrate close tracking with the reference trajectories in both transient and steady-state. The small oscillations in v_{dc} are due to a large proportional gain k_2 . The value of k_2 can be reduced to attenuate the oscillations, however this leads to a slower transition from 200 to 240 V. The controller gains used were $k_1 = 3200 \text{ s}^{-3}$, $k_2 = 8500 \text{ s}^{-2}$, $k_3 = 100 \text{ s}^{-1}$, $k_4 = 300 \text{ s}^{-2}$, $k_5 = 750 \text{ s}^{-1}$. Initial values for the feedback gains were chosen to ensure appropriately fast transient response. That is, for the tracking error subsystem for i_q

$$\begin{bmatrix} \dot{e}_4 \\ \dot{e}_5 \end{bmatrix} = \begin{bmatrix} 0 & 1 \\ -k_4 & -k_5 \end{bmatrix} \begin{bmatrix} e_4 \\ e_5 \end{bmatrix}$$

the gains k_4 and k_5 ensure a settling time of about 10 ms. The gains k_1 , k_2 , k_3 for the 1st tracking error subsystem are chosen to ensure a well damped response with a relatively slow settling time of about 100 ms. This approach led to a reasonable starting point for gain values which were varied a small amount online to account for model error. The control signals are shown in Fig. 6(b) with m_a and δ remaining within their allowed regions.

B. Decoupled Vector Control

In order to compare the performance of the flatness-based control, a traditional vector control method presented in [1] is also implemented on the VSC test stand. The benchmark system

of this approach can be found in [11]. Here, we briefly review this approach. First, we take e_d and e_q as

$$e_d = v_d + L(\omega i_q - p_1), \quad e_q = -L(\omega i_d + p_2) \quad (17)$$

where p_1 , p_2 are outputs of PI compensators for i_d and i_q , respectively. The expressions for p_1 and p_2 are

$$p_1 = k_{id}^p (i_d^*(t) - i_d(t)) + k_{id}^i \int_0^t (i_d^*(\tau) - i_d(\tau)) d\tau$$

$$p_2 = k_{iq}^p (i_q^* - i_q(t)) + k_{iq}^i \int_0^t (i_q^* - i_q(\tau)) d\tau$$

where i_d^* , i_q^* denote reference values. Substituting (17) into (1) gives

$$\frac{di_d}{dt} = -\frac{R_s}{L} i_d + p_1, \quad \frac{di_q}{dt} = -\frac{R_s}{L} i_q + p_2.$$

Hence, we have decoupled stable tracking error dynamics for i_d and i_q . Since the dc voltage in the capacitor is related to the amount of real current entering the VSC, the dc voltage is indirectly controlled with the reference real current i_d^* . Therefore, the output of the PI compensator for the dc voltage is

$$i_d^*(t) = k_v^p (v_{dc}^* - v_{dc}(t)) + k_v^i \int_0^t (v_{dc}^* - v_{dc}(\tau)) d\tau.$$

This control scheme results in cascaded PI compensators for v_{dc} and i_d , where the inner feedback loop controls i_d and the outer feedback loop controls v_{dc} . The i_q control consists of a single PI compensator. Fig. 7 illustrates the block diagram of this approach. The experimental performance of this controller

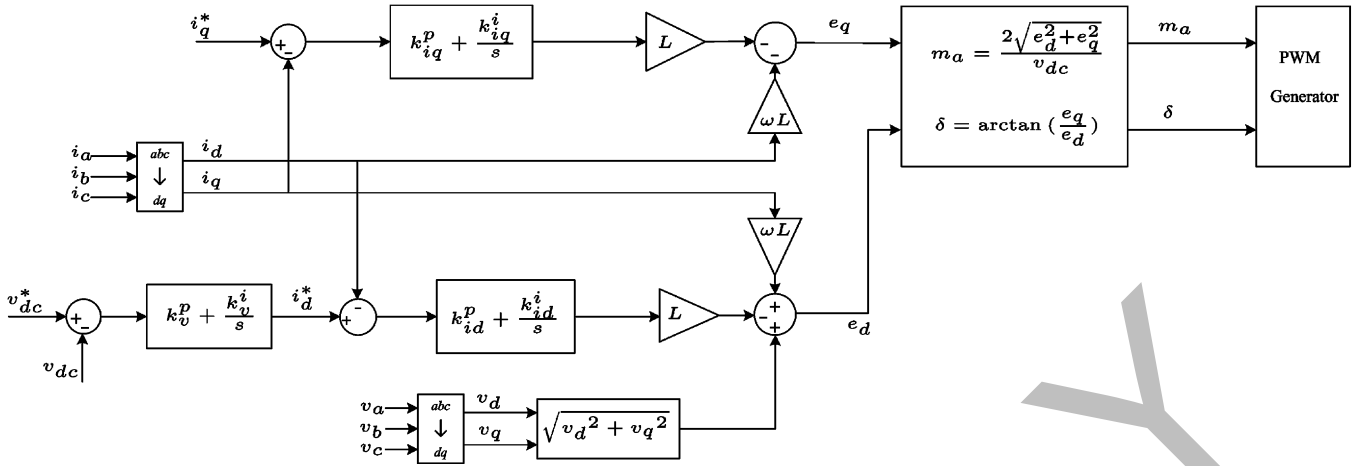


Fig. 7. Block diagram of vector control scheme.

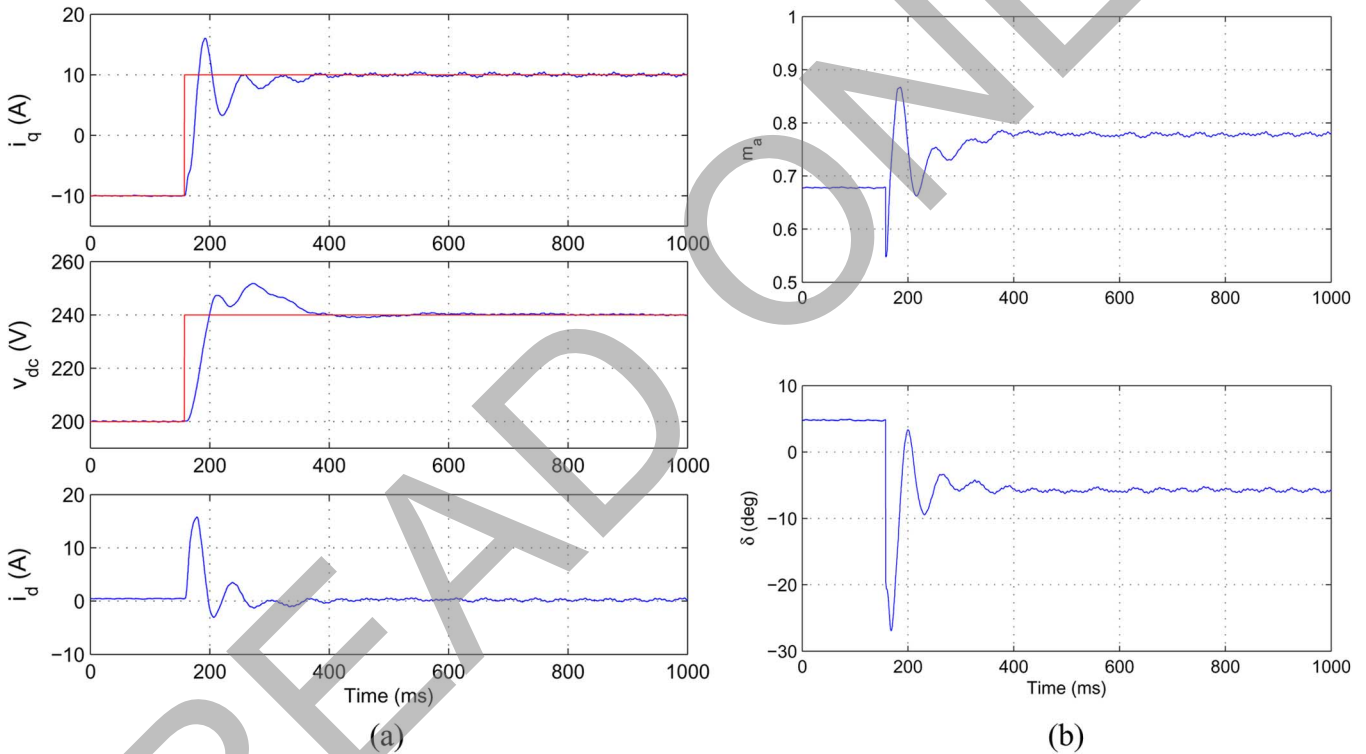


Fig. 8. Vector control for a step change in i_q^* and v_{dc}^* . (a) Trajectory of i_a , v_{dc} , i_q , v_{dc}^* , and i_q^* . (b) Trajectories of m_a and δ .

is shown in Fig. 8, where we perform a transition for i_q from -10 to 10 A and v_{dc} from 200 to 240 V. Unlike in the non-linear control, here the reference trajectories are discontinuous functions of time with a step change occurring at $t = 150$ ms. These results were obtained with controller gains $k_{id}^p = 3$ V/A, $k_{id}^i = 65$ V/(A · s), $k_{iq}^p = 3$ V/A, $k_{iq}^i = 65$ V/(A · s), $k_v^p = 0.54$ A/V, $k_v^i = 10.8$ A/(V · s). These gains were tuned using linear systems theory. For example, letting $\xi_1 = \int_0^t i_d^* - i_d(\tau) d\tau$ and $\xi_2 = i_d^* - i_d$ (with $i_d^* = 0$ for steady state) yields the error system

$$\begin{bmatrix} \dot{\xi}_1 \\ \dot{\xi}_2 \end{bmatrix} = \begin{bmatrix} 0 & 1 \\ -k_{id}^i & -k_{id}^p - \frac{R_s}{L} \end{bmatrix} \begin{bmatrix} \xi_1 \\ \xi_2 \end{bmatrix}.$$

The gains k_{ip}^i and k_{id}^p were chosen for a settling time of approximately 50 ms. The dc voltage controller tuning was performed similarly. Using these gain values as a starting point, the gains were varied a small amount online to improve the measured response.

Comparing Fig. 6(a) and (b) with Fig. 8, the flatness-based controller performs the transition for both i_q and v_{dc} faster and with reduced settling time. The flatness-based controller's transition is smoother, has less oscillation and overshoot. Considerable effort was placed on exhaustively varying the vector controller's gains in order to improve its performance. Although, transient response could be improved relative to that shown in the figures, this improvement came at the expense of reduced stability margin.

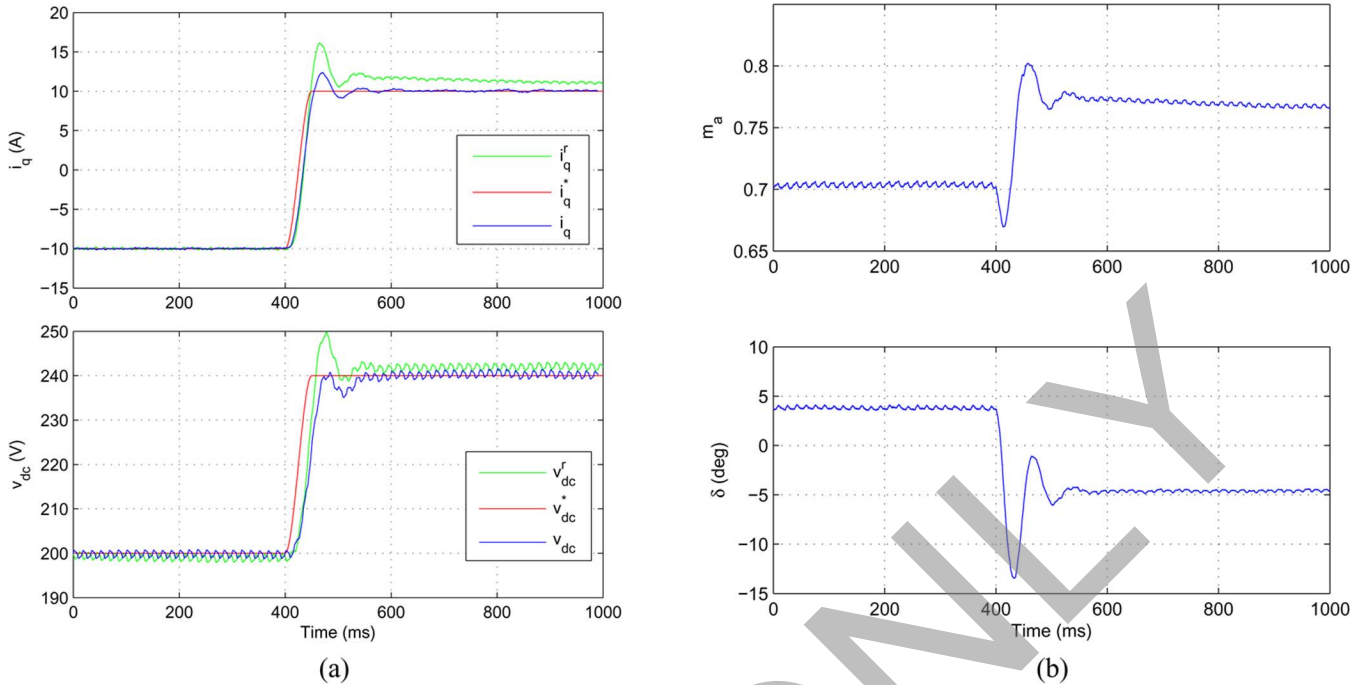


Fig. 9. Robustness of the flatness-based control. (a) Trajectories of i_q , i_q^* , v_{dc} , and v_{dc}^* . (b) Trajectories of m_a and δ ($R_s = 0$, $R_c = \infty$).

C. Robustness of the Flatness-Based Control

Since flatness-based control is model-based, we expect it to have some sensitivity to error in model parameters. In order to evaluate its robustness, the flatness-based control was tested with the lossless parameters case, i.e., $R_s = 0$ and $R_c = \infty$. This corresponds to system with no losses and leads to a significantly less complex expression for the control law. Fig. 9 shows the desired trajectories i_q^* , v_{dc}^* and the actual trajectories i_q , v_{dc} using the more accurate parameters. The plots denoted by i_q^r and v_{dc}^r are the trajectories corresponding to a control based on the assumption $R_s = 0$, $R_c = \infty$. Evidently the performance of the tracking control is affected by the model parameters error considered. However, the system remains stable and the feedback is able to bring i_q , v_{dc} close to their desired values. Other experiments were performed to investigate robustness to a reasonable amount of variation in other model parameters such as L , C , and ω , and satisfactory performance was also obtained in these cases.

The vector control law depends explicitly on a reduced number of parameters: R_s , L , ω , and v_d . Experimental testing demonstrated that errors in these parameters had relatively little affect on tracking performance and we conclude that vector control is relatively robust compared to the proposed flatness-based approach whose increased sensitivity to model error is undoubtedly due to a more complicated dependence on system parameters. Work in [4] presents an I/O linearizing control with tracking output (i_d, i_q) which is quite similar to vector control except in minor details of the inner current control loops. That work also concluded performance is robust; experiments with $\pm 40\%$ change in L and $\pm 15\%$ change in v_d were considered. In [16], the authors show robust simulation results of a vector control augmented by an inductor/capacitor/inductor (LCL)—filter. By adding a filter, oscillations due

to disturbances in the system can be mitigated at the expense of reduced response time. On the other hand, for reasonably accurate parameter values in the proposed nonlinear control, the transient tracking performance was found to be more desirable than that of vector control.

D. Unbalanced Three-Phase AC Voltage Compensation

In this section, we investigate setpoint regulation of the system for an unbalanced ac source. From (2) and (3), we observe that when unbalance is present v_d and v_q contain sinusoidal components with frequency 2ω . In this section, we illustrate regulation of i_q and v_{dc} for the particular unbalance

$$\begin{aligned} v_a &= 100 \cos(\omega t) \\ v_b &= 100 \cos\left(\omega t - \frac{2\pi}{3}\right) \\ v_c &= 90 \cos\left(\omega t + \frac{2\pi}{3} + \frac{\pi}{18}\right) \end{aligned}$$

which gives

$$\begin{aligned} v_d(t) &= 78.56 + 5.23 \cos(2\omega t) - 0.55 \sin(2\omega t) \\ v_q(t) &= 4.25 - 0.55 \cos(2\omega t) - 5.23 \sin(2\omega t). \end{aligned} \quad (18)$$

Unbalance in the ac voltage was created by connecting a single phase variac to a phase. Phase shift can be created by adding inductance to the phase. Substituting (14) into the expressions for u in (9) shows that when the system is at equilibrium the flatness-based open- or closed-loop control will be time-varying due to time-varying v_d and v_q . Fig. 10 shows the experimental response of i_d and i_q . Initially, the system is operating in open-loop assuming $v_d = 100\sqrt{2/3}$, $v_q = 0$ and constant controls $m_a = 0.7$, $\delta = 3^\circ$. This results in oscillations in i_d and i_q with amplitudes of about 2.1 and 2.5 A, respectively. Fig. 10

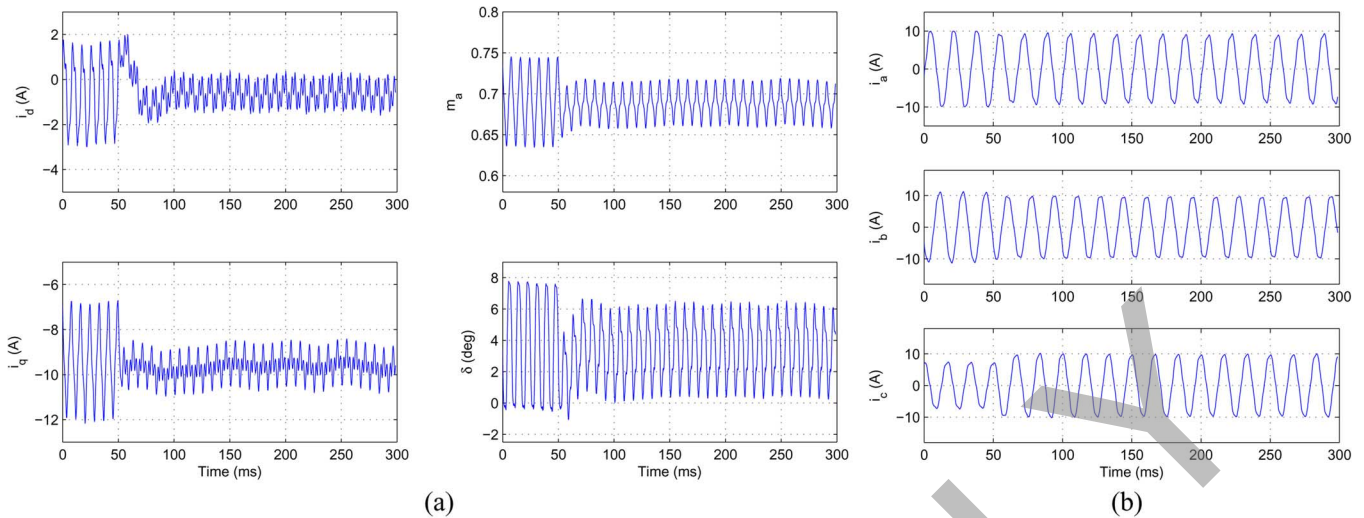


Fig. 10. Engagement of unbalance voltage compensation. (a) Trajectories of i_d , i_q , m_a , and δ . (b) Trajectories of i_a , i_b , and i_c .

shows that m_a and δ are varying with time for $t < 50$ ms. This is because the closed-loop control is being plotted but not applied to the system. At $t = 50$ ms, the closed-loop control is switched on and we observe that oscillations in i_d and i_q are significantly reduced to approximately 0.8 and 1 A, respectively. The figure also shows the corresponding control signals m_a , δ , and three-phase currents i_a , i_b , and i_c . Note that after the control is switched on, the amplitude of i_c increases to balance the three-phase currents.

VII. CONCLUSION

This brief has presented a nonlinear control strategy to achieve trajectory tracking of a PWM VSC. The main contribution of this brief is the implementation and experimental validation of the flatness-based control technique which allows open-loop motion planning. A flatness-based control has been successfully implemented on an actual VSC test stand. Open-loop motion planning is used to steer the system between equilibria while respecting input constraints. Closed-loop control ensures that tracking is robust to model error, initial tracking error, and disturbances. Experimental results illustrate that the nonlinear control provides improved transient tracking performance relative to a traditional vector control method. An unbalanced ac source was considered and the flatness-based control was validated experimentally for setpoint regulation.

REFERENCES

- [1] C. Schauder and H. Mehta, "Vector analysis and control of advanced static VAR compensators," *IEE Proc.-C*, vol. 140, no. 4, pp. 299–306, Jul. 1993.
- [2] P. W. Lehn, "Exact modeling of the voltage source converter," *IEEE Trans. Power Delivery*, vol. 17, no. 1, pp. 217–222, Jan. 2002.
- [3] P. Rioual, H. Pouliquen, and J. P. Louis, "Nonlinear control of PWM rectifier by state feedback linearization and exact PWM control," in *Proc. IEEE Power Electron. Specialists Conf. Rec. (PESC)*, Taipei, Taiwan, Jun. 1994, pp. 1095–1102.
- [4] T.-S. Lee, "Input-output linearization and zero-dynamics control of three-phase AC/DC voltage-source converters," *IEEE Trans. Power Electron.*, vol. 18, no. 1, pp. 11–22, Jan. 2003.
- [5] D.-C. Lee, G.-M. Lee, and K.-D. Lee, "DC-bus voltage control of three-phase AC/DC PWM converters using feedback linearization," *IEEE Trans. Ind. Appl.*, vol. 36, no. 3, pp. 826–833, May/June 2000.
- [6] A. Gensior, J. Rudolph, and H. Güldner, "Flatness based control of three-phase boost rectifiers," presented at the 11th Eur. Conf. Power Electron. Appl. Rec. (EPE), Dresden, Germany, Sep. 2005.
- [7] Powerex Inc., Youngwood, PA, "Powerex Data Sheet, T120," 2005. [Online]. Available: www.pwr.com
- [8] N. Mohan, T. Undeland, and W. Robbins, *Power Electronics: Converters, Applications, and Design*. New York: Wiley, 2003.
- [9] Opal-RT Technologies, Montreal, QC, Canada, "RT-LAB Version 8 user guide," 2005. [Online]. Available: www.opal-rt.com
- [10] V. Dinavahi, R. Iravani, and R. Bonert, "Design of a real-time digital simulator for a D-STATCOM system," *IEEE Trans. Ind. Electron.*, vol. 51, pp. 1001–1008, Oct. 2004.
- [11] C. K. Sao, P. W. Lehn, M. R. Iravani, and J. A. Martinez, "A benchmark system for digital time-domain simulation of a pulse-width-modulated D-STATCOM," *IEEE Trans. Power Delivery*, vol. 17, no. 4, pp. 1113–1120, Oct. 2002.
- [12] E. Song, "Experimental validation of a flatness-based control for a voltage source converter," M.S. thesis, Dept. Elect. Comput. Eng., Univ. Alberta, Edmonton, AB, Canada, 2006.
- [13] P. Martin, R. M. Murray, and P. Rouchon, "Flat systems, equivalence and feedback," in *Advances in the Control of Nonlinear Systems*, A. Baños, F. Lamnabhi-Lagarigue, and F. J. Montoya, Eds. New York: Springer-Verlag, 2001, vol. 264, pp. 3–32.
- [14] B. Charlet, J. Lévine, and R. Marino, "On dynamic feedback linearization," *Syst. Control Lett.*, vol. 13, pp. 143–151, 1989.
- [15] R. Marino and P. Tomei, *Nonlinear Control Design: Geometric, Adaptive, and Robust*. Hertfordshire, U.K.: Prentice-Hall, 1995.
- [16] M. Bongiorno and J. Svensson, "Voltage dip mitigation using shunt-connected voltage source converter," *IEEE Trans. Power Electron.*, vol. 22, no. 9, pp. 1867–1874, Sep. 2007.